Supporting Information

Room-temperature synthesis of Zr-UiO-66 metal-organic frameworks via mechanochemical pretreatment for the rapid removal of EDTA-chelated copper from water

Yi-nan Wu, [a,b], Junyi Cai [a,b], Shuliang Hou [a,b], Rui Chen, [a,b], Ziqi Wang [a,b], Daniel Manaye Kabtamu [c],Osman Ahmed Zelekew [a,b,d], and Fengting Li [a,b,]*

a.College of Environmental Science and Engineering, State Key Laboratory of Pollution Control and Resource Reuse, Tongji University, Shanghai 200092, P.R. China

b.Shanghai Institute of Pollution Control and Ecological Security, Shanghai 200092, P.R. China

E-mail: fengting@tongji.edu.cn

c. Department of Chemistry, Debre Berhan University, 445, Debre Berhan, Ethiopia

d. Department of Materials Science and Engineering, Adama Science and Technology University, Adama 1888, Ethiopia

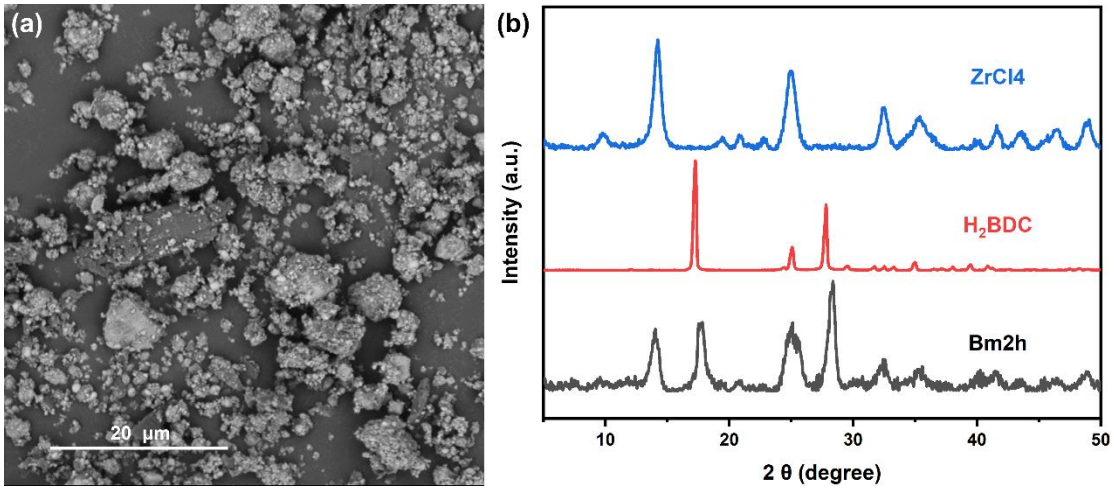

Figure S1. SEM image (a) and XRD patterns (b) of reactive mixture after ball milling.

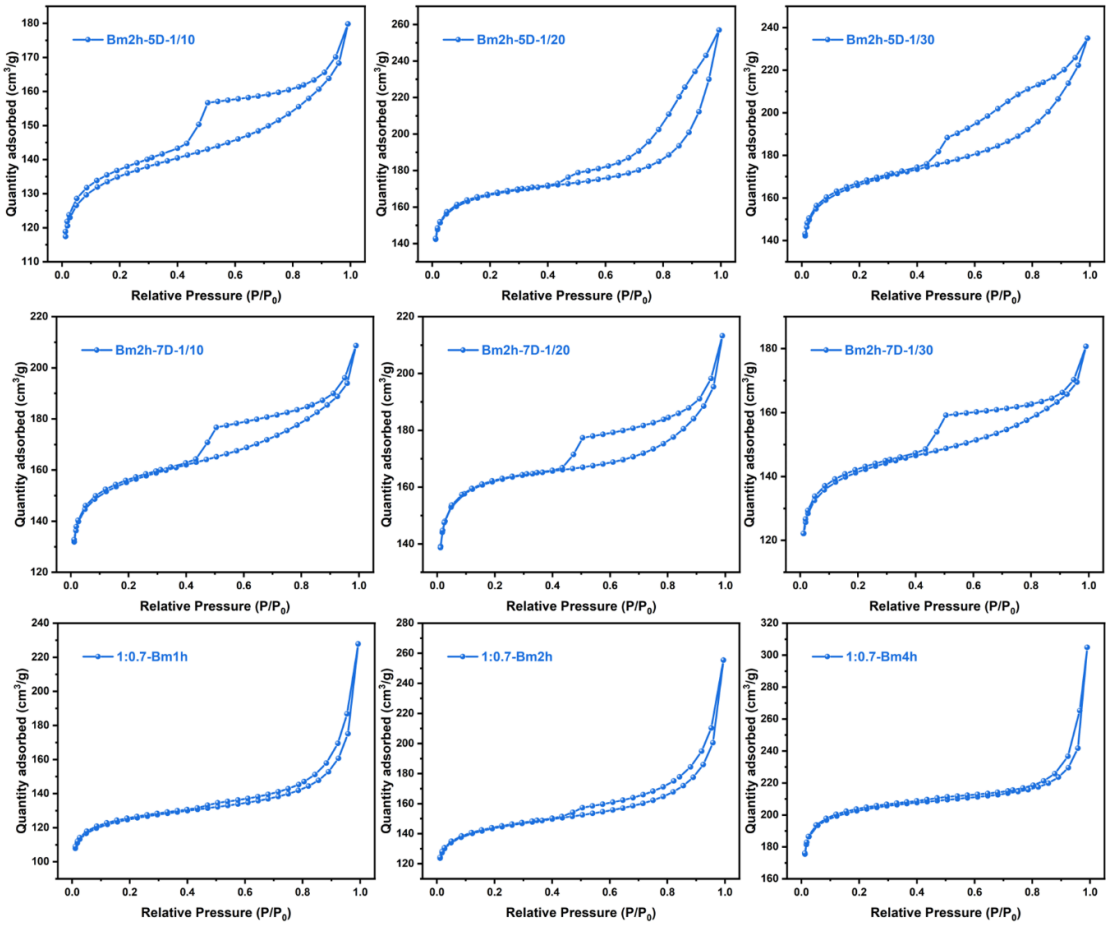

Figure S2. N_2 sorption isotherm of UiO-66(Zr) obtained under different synthetic conditions.

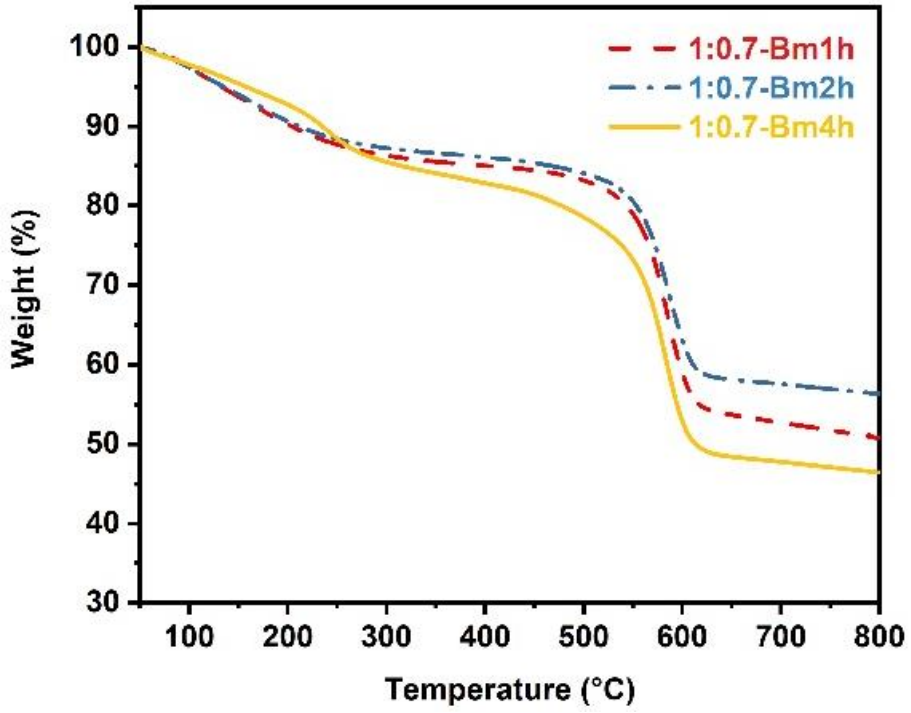

Figure S3. TGA curves of as-synthesized UiO-66(Zr) under optimized synthetic conditions (1:0.7) at different ball milling pretreatment durations.

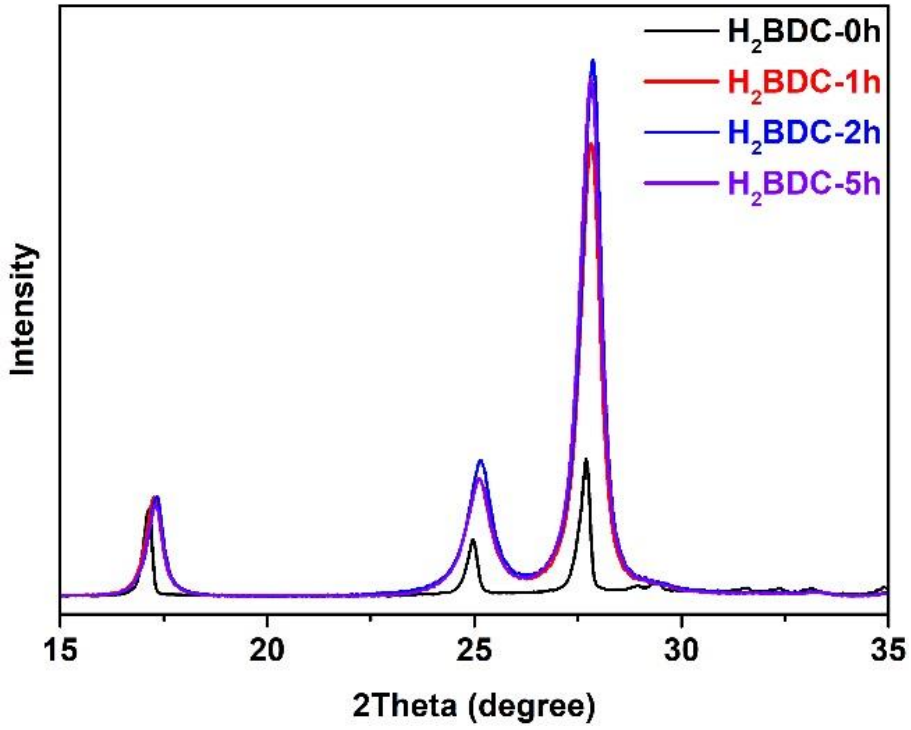

Figure S4. XRD patterns of terephthalic acid for different ball-milling time.

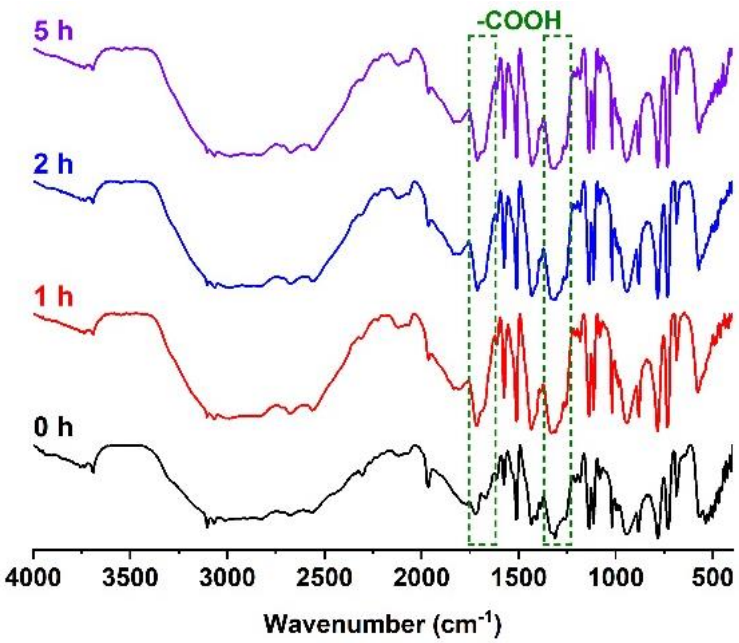

Figure S5. FT-IR patterns of terephthalic acid for different ball milling hours.

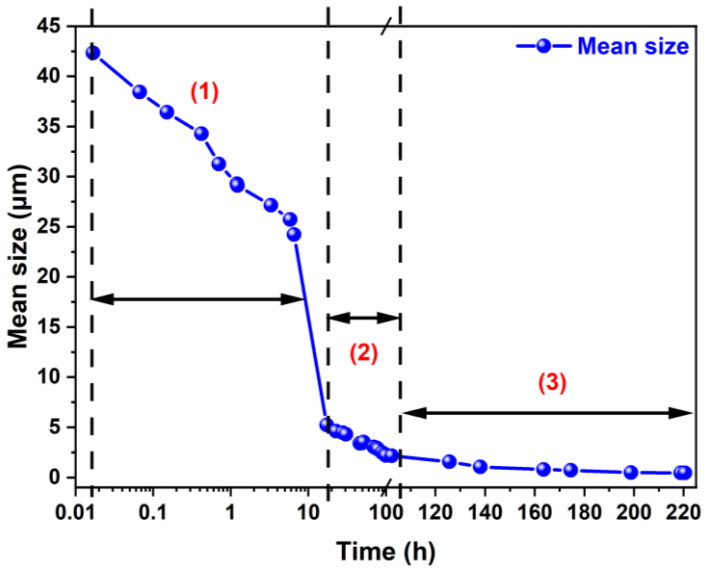

Figure S6. Temporal evolution of mean particle size during the synthesis. The pattern of the mean particle size change corresponds to three stages of the ethanol phase reaction: (1) initial dispersion (0–10 h), (2) mid-term release (10–100 h), and (3) late growth (100-220 h).

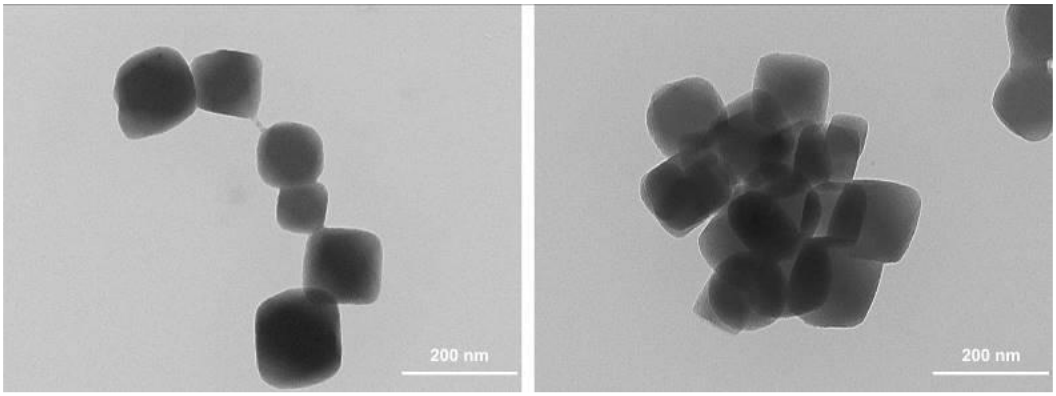

Figure S7. TEM images of UiO-66(Zr)-mw.

Table S1. Textural properties of UiO-66(Zr)-rm and UiO-66(Zr)-mw.

Sample	S_{BET} (m^2/g)	$S_{Langmuir}$ (m^2/g)	V_{micro} (cm^3/g)	V_{meso} (cm^3/g)	V_T (cm^3/g)
UiO-66(Zr)-mw	1122.5	1244.5	0.378	0.228	0.487
UiO-66(Zr)-rm	709.8	898.7	0.180	0.500	0.680

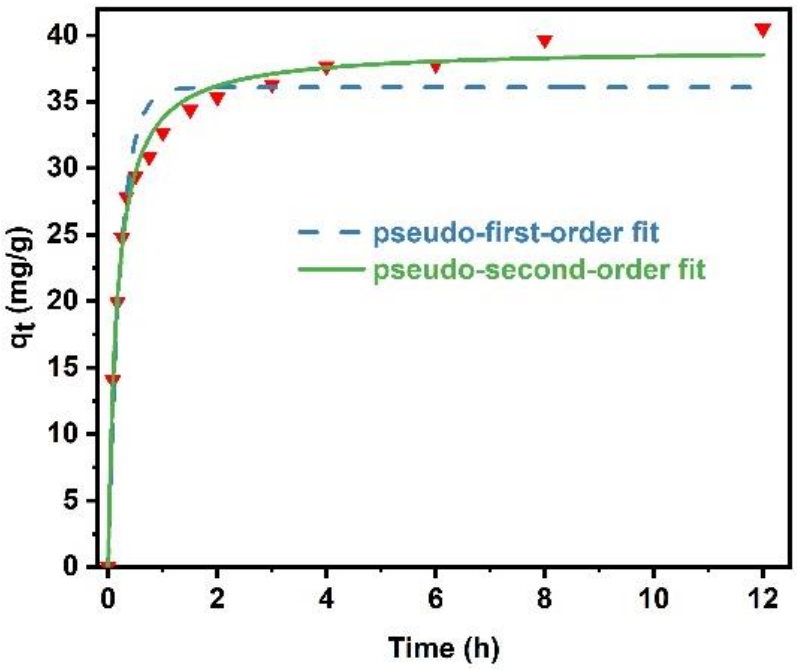

Figure S8. Adsorption kinetics of EDTA-Cu^{II} on UiO-66(Zr)-rm.

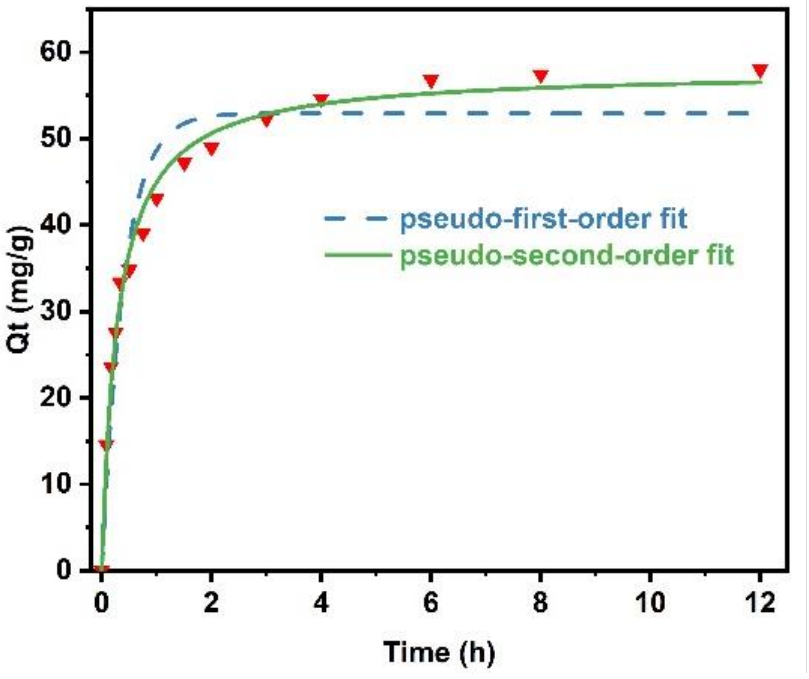

Figure S9. Adsorption kinetics of EDTA-Cu^{II} onto UiO-66(Zr)-mw

Table S2. Comparison of the key parameters for the adsorptive removal of Cu-EDTA between UiO-66(Zr)-mw, UiO-66(Zr)-rm and other reported sorbents

Adsorbent	BET Surface Area (m^2/g)	Testing pH	Initial Concentration (mg/L)	Langmuir Model Adsorption Capacity(mg/g)	Pseudo Second Order k^2 (g/(mg·min))	Reference
UiO-66(Zr)-rm	710	6	10	39	0.16	This work
UiO-66(Zr)-mw	1123	6	10	58	0.06	This work
Amino-Functionalized Mesoporous Silica	295	5.5	35.2	26.3	-	[1]
Granular Activated Carbon	1000	5	111	8.9	-	[2]
Green Rust	78	8	128	126	0.008	[3]
Fe/Zr pillared Montmorillonite	121	6	20	15.5	0.12	[4]
Chitosan	94.7	5	45.9	19.7	-	[5]

Table S3. The kinetic parameters for the adsorption of EDTA-Cu^{II} on UiO-66(Zr)-rm and UiO-66(Zr)-rm.

Adsorbent	Pseudo first order			Pseudo second order		
	k_1	q_e	R^2	k_2	q_e	R^2
UiO-66(Zr)-rm	4.44	36.09	0.951	0.16	39.04	0.991
UiO-66(Zr)-mw	2.52	52.94	0.941	0.06	57.87	0.990

Table S4. Modeling parameters obtained by fitting of Langmuir and Freundlich equation.

Adsorbent	Langmuir			Freundlich		
	q_m	b	R^2	K_f	n	R^2
UiO-66(Zr)-rm	43.13	11.90	0.931	33.02	7.83	0.893

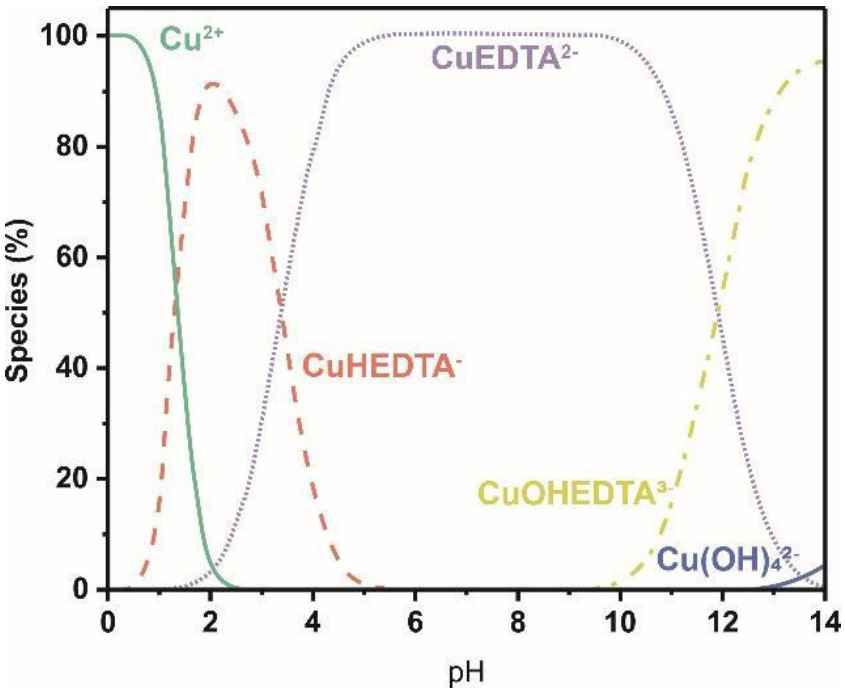

Figure S10. Distribution of EDTA-Cu^{II} species under different pH.

References

1 Wu, L.; Wang, H.; Lan, H.; Liu, H.; Qu, J. *Sep. Purif. Technol.* 2013, **117**, 118-123.

2 Chu, K. H.; Hashim, M. A. *J. Chem. Technol. Biotechnol.* 2000, **75** (11), 1054-1060.

3 Wang, L.; Luo, Z.; Chelme-Ayala, P.; Wei, J.; Zhou, X.; Min, Y.; Gamal El-Din, M.; Wu, Z. *J. Environ. Manage.* 2021, **279**, 111516.

4 Wu, P.; Zhou, J.; Wang, X.; Dai, Y.; Dang, Z.; Zhu, N.; Li, P.; Wu, J. *Desalination* 2011, **277** (1), 288-295.

5 Juang, R.-S.; Ju, C.-Y. *Ind. Eng. Chem. Res.* 1997, **36** (12), 5403-5409.